Int. J. Heat Mass Transfer. Vol. 36, No. 12, pp. 2997–3007, 1993
Printed in Great Britain

0017–9310/93 $6.00+0.00


# Theory and measurement of local interfacial area using a four sensor probe in two-phase flow

S. T. REVANKAR and M. ISHII†
School of Nuclear Engineering, Purdue University, West Lafayette, IN 47907, U.S.A.

(*Received* 23 *June* 1992 *and in final form* 5 *January* 1993)

**Abstract**—A theoretical foundation of the measurement method for the time averaged local interfacial area using a four sensor resistivity probe is presented. Based on this theory, the four sensor resistivity probe was developed and employed to measure the interfacial velocity, local interfacial area concentration and void fraction in a vertical air–water cap bubbly flow. The four sensor probe measurements were checked against the global void measurement using a differential pressure. The results were very satisfactory. Theoretical profiles of the void fraction and interfacial area concentration were obtained using the pictures of cap bubbles. The theoretical predictions of the cap bubbles and the interfacial area concentration profiles compared very well with the four sensor data.

## 1. INTRODUCTION

TO MODEL a two-phase flow system accurately detailed information on the internal flow structure is required. The mean characteristics of the internal structure of the two-phase flow can be described by two geometrical parameters, the void fraction and the interfacial area concentration. The void fraction represents the volumetric fraction or the probability density for a phase to exist at a given time and point, whereas the interfacial area represents the available surface area for phases to coexist and/or interact. The latter parameter is particularly important in determining the rate of mass, momentum and energy transfer between phases or components. These parameters are used in the two-phase flow models such as the drift flux model and two-fluid model [1, 2]. For example, the gas–liquid interfacial area is an important factor which affects the reactivity of the gas–liquid reaction in the metallurgical processes such as ladle refining and vacuum oxygen decarburization [3]. In the two-fluid model the interfacial transfer terms describing the transfer of mass, momentum and energy can be expressed as the product of the local specific interfacial area and the driving force [1]:

$$\text{Interfacial transfer term} = \text{Driving force} \times \frac{1}{L_s}. \quad (1)$$

The driving forces are characterized by the local transport mechanisms such as molecular and turbulent diffusions whereas the local specific interfacial area $1/L_s$, is related to the structure of the two-phase flow field. Experimental data on the local interfacial area concentration are very scarce. Most of the available experimental data are limited to the volume averaged interfacial area concentration over a section of a flow channel. Furthermore, there are very few established theoretical foundations for relating this interfacial area to some easily measurable quantities. Especially for flow regimes other than bubbly flow no established method of a local measurement of the interfacial area exists. In this paper a four sensor resistivity probe method for the measurement of the interfacial area concentration and the void fraction is presented. As a test of the present method a cap bubbly flow regime was studied in a vertical air–water flow system. This regime was chosen for bench marking this instrumentation method, because the interfacial area data can also be obtained photographically with high accuracy.

## 2. THEORY OF LOCAL INTERFACIAL AREA MEASUREMENT FOR FOUR SENSOR PROBE

By considering a moving gas–liquid interface $j$ which is represented by $f_j(x, y, z, t) = 0$, the local instantaneous interfacial area concentration is given in terms of distribution [1]:

$$a_i(x, y, z, t) = \sum_j |\vec{\nabla} f_j| \delta(f_j(x, y, z, t)). \quad (2)$$

This formulation is valid for any flow regime of two-phase flow.

Since the distribution, $\delta(f_j(x, y, z, t))$, is not observable experimentally, the time averaged value of interfacial area concentration is more practical. By averaging equation (2) in time duration $\Omega$ at $x_0$, $y_0$ and $z_0$, the time averaged local interfacial area concentration is given by [1, 4, 5],

$$\bar{a}_i'(x_0, y_0, z_0) = \frac{1}{\Omega} \sum_j \left\{ |\vec{\nabla} f_j| \Big/ \left| \frac{\partial f_j}{\partial t} \right| \right\} \text{ at } (x_0, y_0, z_0, t_j) \quad (3)$$

† Author to whom correspondence should be addressed.

## NOMENCLATURE

$a_i$ interfacial area concentration
$a_i(x, y, z, t)$ local instantaneous interfacial area concentration
$\bar{a}_i^t$ time averaging of $a_i(x, y, z, t)$
$A_0$–$A_3$ determinants given by equations (15) and (17)
$c_1, c_2$ limits on transit time to discriminate small and cap bubbles
$\cos\eta_{xk}, \cos\eta_{yk}, \cos\eta_{zk}$ direction cosines of $\vec{n}_{sk}$
$f_j(x, y, z, t)$ function representing $j$th interface
$h$ cap bubble height
$j_g, j_f$ superficial velocity of gas and liquid
$l_d$ distance between two adjacent rear sensors
$L_B$ cap bubble length
$L_s$ length scale at interface
$n$ number
$\vec{n}_j$ unit normal vector of $j$th interface
$\vec{n}_s$ unit vector in the direction of probe
$\vec{n}_{sk}$ unit vector in the direction of $k$th sensor
$N_c$ number of cap bubbles passing a point per unit time
$N_s$ number of small bubbles passing a point per unit time
$r$ distance from the center to pipe wall
$R$ pipe radius
$s_p$ projected area of the probe in the flow direction
$t$ time
$t_j$ time when $j$th interface passes the probe
$\vec{v}_{ij}$ velocity of $j$th interface
$v_{skj}$ passing velocity of $j$th interface with respect to rear sensor $k$
$V_B$ velocity of cap bubble
$x, y, z$ coordinates
$x_k, y_k, z_k$ coordinates of rear sensor $k$
$x_0, y_0, z_0$ fixed point in $x$, $y$ and $z$ coordinate system.

Greek symbols
$\alpha$ void fraction of gas phase
$\delta(x)$ delta function
$\Delta s$ spacing between tip and rear sensor of double probe
$\Delta t_{kj}$ transit time for $j$th interface to pass between front and rear sensor $k$
$\xi_j$ angle between $\vec{n}_s$ and $\vec{n}_j$
$\tau$ reciprocal of number of interfaces passing a point per unit time
$\phi_j$ angle between $\vec{n}_j$ and $\vec{v}_{ij}$
$\Omega$ time duration.

Subscripts
f, g, i liquid phase, gas phase, value at interface
$j$ interface number
$k$ rear sensor number ($k = 1, 2, 3$)
0 reference.

for all $j$ satisfying $t < t_j < t+\Omega$. With $\phi_j$ as the angle between the velocity of the $j$th interface, $\vec{v}_{ij}$, and the direction of the surface normal vector at $(x_0, y_0, z_0, t_j)$ (see Fig. 1(a)), the following relation can be obtained

$$|\vec{\nabla} f_j| \Big/ \left|\frac{\partial f_j}{\partial t}\right| = \frac{1}{|\vec{v}_{ij}| \cos\phi_j}. \tag{4}$$

From equations (3) and (4) one gets

$$\bar{a}_i^t(x_0, y_0, z_0) = \frac{1}{\Omega} \sum_j \frac{1}{|\vec{v}_{ij}| \cos\phi_j}. \tag{5}$$

Now $j$ is arranged such that $t_j$ is in increasing order as $t_{j-1} < t_j < t_{j+1}$. Then by assuming the following uniformity of the time intervals

$$\frac{1}{2n+1} \sum_{j=-n}^{n} |t_{j+1} - t_j| = \tau \tag{6}$$

one obtains the following relation for a large value of $\Omega$,

$$\left(\sum_j\right) = \Omega/\tau. \tag{7}$$

Substituting equation (7) into equation (5) and using the symbol for a mean value,

$$\bar{a}_i^t(x_0, y_0, z_0) = \frac{1}{\tau} \overline{\frac{1}{|\vec{v}_i| \cos\phi}}. \tag{8}$$

Here the reciprocal of a harmonic mean of $|\vec{v}_{i,j}| \cos\phi_j$ is given by

$$\overline{\frac{1}{|\vec{v}_i| \cos\phi}} = \sum_j \frac{1}{|\vec{v}_{ij}| \cos\phi_j} \Big/ \left(\sum_j\right). \tag{9}$$

Now consider a four sensor probe shown in Fig. 1(b). The unit vector $\vec{n}_{sk}$ and its direction cosines for rear sensor $k$ are represented by $(\cos\eta_{xk}, \cos\eta_{yk}, \cos\eta_{zk})$, with $k = 1, 2, 3$. The position of the tip sensor is given by $(x_0, y_0, z_0)$. The position of the rear sensor $k$ is given by $(x_k, y_k, z_k)$, where $x_k$, $y_k$ and $z_k$ are given by

$$\begin{aligned} x_k &= x_0 + \Delta s_k \cos\eta_{xk} \\ y_k &= y_0 + \Delta s_k \cos\eta_{yk} \quad k = 1, 2, 3. \\ z_k &= z_0 + \Delta s_k \cos\eta_{zk} \end{aligned} \tag{10}$$

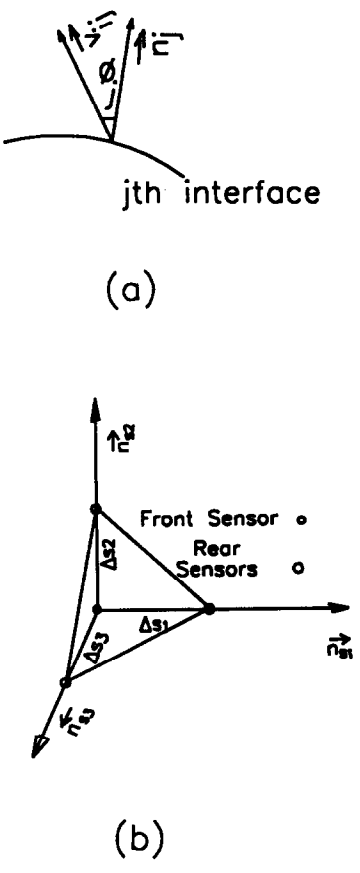


FIG. 1. (a) Angle between $\vec{v}_{ij}$ and $\vec{n}_j$; (b) Schematic of a four sensor probe.

By considering the $j$th interface passing the front sensor and rear sensor $k$, with the time interval, $\Delta t_{kj}$, the passing velocity, $v_{skj}$ is given by

$$v_{skj} = \frac{\Delta s_k}{\Delta t_{kj}}, \quad k = 1,2,3. \tag{11}$$

As the $j$th surface is represented by $f_j(x,y,z,t)$, the surface equation should satisfy

$$f_j(x_0, y_0, z_0, t_j) = 0 \tag{12}$$

$$f_j(x_k, y_k, z_k, t_j + \Delta t_{kj}) = 0, \quad k = 1,2,3 \tag{13}$$

where $t_j$ is the time when the $j$th interface passes the front sensor. When the distance $\Delta s_k$ and the time difference $\Delta t_{kj}$ are small compared to the length scale and time scale, respectively, then we have from equations (10) and (11) the following relation

$$\frac{\partial f_j}{\partial x}\cos\eta_{xk} + \frac{\partial f_j}{\partial y}\cos\eta_{yk} + \frac{\partial f_j}{\partial z}\cos\eta_{zk} = -\frac{\partial f_j}{\partial t}\frac{1}{v_{skj}}, \quad k = 1,2,3. \tag{14}$$

When the unit vectors $\vec{n}_{s1}$, $\vec{n}_{s2}$ and $\vec{n}_{s3}$ are linearly independent then the determinant $|A_0|$ will satisfy

$$|A_0| \equiv \begin{vmatrix} \cos\eta_{x1}, & \cos\eta_{y1}, & \cos\eta_{z1}, \\ \cos\eta_{x2}, & \cos\eta_{y2}, & \cos\eta_{z2}, \\ \cos\eta_{x3}, & \cos\eta_{y3}, & \cos\eta_{z3}, \end{vmatrix} \neq 0. \tag{15}$$

Under the condition of non-vanishing determinant given by equation (15), equation (14) has a solution from which it can be shown that

$$(|\vec{v}_{ij}|\cos\phi_j)^{-1} = \frac{\sqrt{(|A_1|^2 + |A_2|^2 + |A_3|^2)}}{\sqrt{(|A_0|^2)}}, \tag{16}$$

where the determinant $|A_1|$ is given by

$$|A_1| \equiv \begin{vmatrix} \frac{1}{v_{s1j}}, & \cos\eta_{y1}, & \cos\eta_{z1}, \\ \frac{1}{v_{s2j}}, & \cos\eta_{y2}, & \cos\eta_{z2}, \\ \frac{1}{v_{s3j}}, & \cos\eta_{y3}, & \cos\eta_{z3}, \end{vmatrix}. \tag{17}$$

Similarly $|A_2|$ and $|A_3|$ are given by replacing the second and third column of the determinant $|A_0|$ by the inverse of velocity components.

Now from equations (16) and (5) the time averaged interfacial area concentration is given by

$$\bar{a}_i^t = \frac{1}{\Omega}\sum_j \frac{\sqrt{(|A_1|^2 + |A_2|^2 + |A_3|^2)}}{\sqrt{(|A_0|^2)}}. \tag{18}$$

Thus the local time averaged interfacial area concentration can be measured by three interfacial velocity components and the known geometric parameters of the four sensor probe. The front sensor and three rear sensors of the four sensor probe can be arranged such that they make an orthogonal system. For example, by choosing $x$, $y$ and $z$ as the directions of the line passing through the front to rear sensors 1, 2 and 3, then the above relation equation (18) can be simplified to

$$\bar{a}_i^t = \frac{1}{\Omega}\sum_j \left\{\left(\frac{1}{v_{s1j}}\right)^2 + \left(\frac{1}{v_{s2j}}\right)^2 + \left(\frac{1}{v_{s3j}}\right)^2\right\}^{1/2}. \tag{19}$$

## 3. FOUR SENSOR RESISTIVITY PROBE METHOD

### 3.1. *Principle of measurement*

The electrical resistivity probe technique was proposed first by Neal and Bankoff [6] for the determination of the bubble size and velocity in gas–liquid bubbly flows. Since then various investigators have used two-sensor probes for measurement of two-phase flow parameters. This technique is based on the instantaneous measurement of local electrical resistivity around a sensor in the two-phase system by a two sensor electrode. Sensors are made of an exposed tip of an otherwise electrically insulated metal wire. Basically each sensor works independently as an identifier of a phase surrounding that tip. As the circuit is opened or closed depending on whether the sensor is in contact with the gas or liquid, the voltage drop

across the sensor fluctuates between two reference voltages. From the timing of the shift in the voltage, the time when the gas–liquid interface passes the sensor can be recorded. Therefore, two parallel and independent types of information related to the phase identification and the passing time of the gas–liquid interface are obtained through the signal conditioner from two closely located sensors, which can be used to estimate the void fraction and interface velocity.

A theoretical study carried out at Argonne National Laboratory [5] gives a method of using the electrical resistance probe technique to measure the local interfacial area concentration. Using this theoretically supported method Kataoka *et al.* [4, 5, 7], Wang and Kocamustafaogullari [8], and Revankar and Ishii [9] studied the local interfacial area concentration in air–water bubbly flow using a two sensor resistivity probe. When using the two sensor probe to measure the local interfacial area, it is necessary to make certain statistical assumptions on the distribution of bubble parameters. The ANL study [5] also proposed a four sensor probe to measure the local interfacial area concentration. This method using a four sensor probe does not require any statistical assumptions. Multisensor probes have been used by Burgess and Calderbank [10–12], and Buchholz *et al.* [13] to measure the bubble size and velocity in bubble columns of interest to chemical engineering. These authors used the average void fraction and the mean Sauter diameter measured from these multisensor resistivity probe to find the average interfacial area concentration in bubbly flow. Recently Kataoka and Serizawa [14] have proposed a correlative method for the four sensor probe to measure the interfacial area and presented some preliminary measurements on air–water bubbly flow using this method. In this method the interfacial area is obtained from the measured correlation function of the characteristic functions at two different positions defined by probe sensors. In the present study the theoretical basis of the measurement with the four sensor probe is given in Section 2. Referring to Fig. 1(b) the front sensor makes the common sensor. The rear three sensors along with the common sensor each make a double-sensor probe. Thus there are three double-sensor probes enabling the measurement of velocity components in three directions.

### 3.2. *Four sensor probe design*

A typical design of the four sensor resistivity probe is shown in Fig. 2(a). The material for the probe conductor is platinum wire with a diameter of 0.12 mm. The platinum wire was first coated with GE No. 7031 adhesive and insulating varnish and was then inserted into a 0.2 mm ID thin teflon sleeve. This teflon tube containing the sensor was then inserted into a 0.48 mm ID × 0.68 mm OD stainless steel tube. The ss tube gives material strength and also helps position the sensor tips. Four such ss tubes were inserted in a tube with a diameter of 2 mm. High strength epoxy resin was used in cementing these tubes. The three rear sensor locations were positioned such that the tip of these sensors were on one plane and they were placed axisymmetrically with respect to the central front sensor. Typical vertical distance between the front and rear sensor was 4 mm. The locations of the four sensors were arranged such that the tips of the sensors make an orthogonal coordinate system with the front sensor in the apex and three rear sensors at the rear plane perpendicular to the flow direction. The other end of each probe sensor electrode was connected to a four wire electrically sheathed cable. The whole probe assembly was put in a 3.175 mm tube which has a 90° elbow bend. A high strength epoxy resin cement was used to hold one tube to another. The probe tips were left exposed and a final coating of epoxy resin was applied to insulate the rest of the probe conductor electrodes.

It is very difficult to exactly locate the sensor tips to get an orthogonal system. Hence the direction cosines of the sensor tips were obtained. For this, accurate distances between each sensor tip are required. These lengths were measured by projecting the magnified image of the sensors on a screen using a classroom overhead projector. Any two sensor tips can be focussed with the projector by placing them in the same plane perpendicular to the light path. The distance measured between two sensor tips thus, were accurate with an error less than 0.5%. The mathematical expressions relating the sensor distances and the direction cosines are given in Appendix A.

### 3.3. *Signal processing*

The signal from each sensor contains basically two types of information, namely (i) identification of phase (gas and liquid) and (ii) residence time of each phase (gas or liquid). As indicated in the design of the typical four sensor probe, the front sensor is in the upstream of the flow direction with reference to the three rear sensors which are in the plane perpendicular to the flow direction. For the measurement of void fraction, the signal from any one of the four sensors can be used. However, due to finite size of the probe, the signal from the front sensor was used to represent the local void fraction. A typical output from a four sensor probe is shown in Fig. 2(b) for spherical cap bubbly flow. The conditioned signal consists of square waves, where the number of squares gives the number of bubbles and the width of the square gives the bubble residence time. From this information the time averaged local void fraction is obtained.

While employing this four sensor probe the following four important factors were noted.

(1) The probe size should be small such that the interfacial curvature effect on the three dimensional measurement is not significant. To minimize this limitation the probe was studied in a vertical cap bubbly flow system where the cap bubble size is large compared with the probe size.

(2) A passing interface should be properly ident-

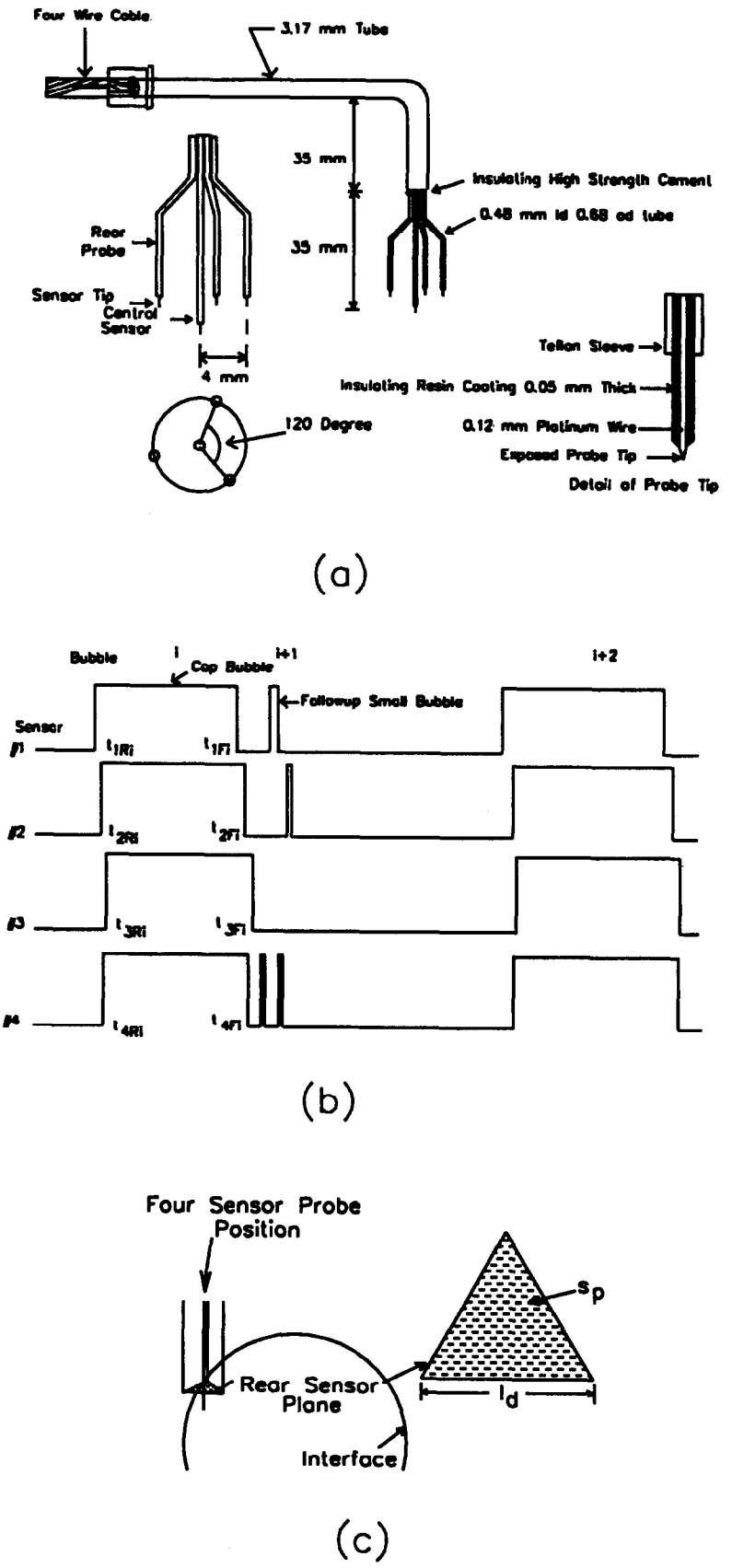


FIG. 2. (a) Design of typical four sensor resistivity probe; (b) Typical output of four sensor probe in cap bubbly flow; (c) Projection of rear sensors plane and location of probe for missing interface.

ified. When there are different sized bubbles, as in the present work the cap bubbles and the small spherical follow-up bubbles should be identified separately. For this the bubble residence time on the front sensor was used to identify the cap bubbles from the smaller tail bubbles. Denoting the rise and fall times of the four sensor signals as $t_{kR}$, and $t_{kF}$, $k = 1, 2, 3, 4$; the following condition on bubble residence time was used to discriminate cap and small bubbles;

$$c_1 \leqslant t_{1R} - t_{1F} \leqslant c_2 \tag{20}$$

where $c_1$ and $c_2$ are time constants determined by the calibration process where the cap bubble size is estimated with flow visualization.

(3) The same interface should pass all the four sensors. In the present method three passing velocities must be measured for the same interface to estimate the interfacial area. However, because of the finite size of the probe some interfaces contact the front sensor and escape from the one or more of the rear sensors and vice versa. This phenomena was also observed by Kataoka and Serizawa [14]. Typically when the location of the probe was near the pipe wall, one of the rear sensors would not detect any interface. This indicated that if the interface was detected by the central front sensor, the interface should have close to vertical orientation between the front sensor and the rear sensor which did not detect the interface. The contribution of the interfacial area from such an interface would be substantial and must be accounted for. For such missing interfaces the interfacial area concentration was estimated with special mathematical formula. The basic idea was to use the projected area of the probe in the flow direction $s_p$, the distance between two downstream sensors $l_d$, and the residence time $\tau_b$ (see Fig. 2(c)) to define the interfacial area for this $j$th interface as

$$a_j = \frac{\tau_b}{\Omega} \frac{l_d}{s_p}. \tag{21}$$

(4) Deformation of the interface by the probe sensors may be significant. Since there are four sensors contacting the interface, the interface deformation is expected to be more pronounced than for the two sensor probe. The effects of the probe-interface interaction and the probe response in relation to wettability and signal to noise ratio are being studied in detail in a separate study. However, in the present experiment, the direct photographic study indicated that this effect was small.

## 4. EXPERIMENTAL APPARATUS

A schematic diagram of the apparatus for the cap bubble column experiment is shown in Fig. 3. The test section is made of lucite pipe. The height of the test pipe is 1.5 m and its inside diameter is 0.0508 m. The bubble generator was made of 49 stainless steel hypodermic tubes of ID 0.12 mm. The tubes were arranged in the $7 \times 7$ square matrix with the pitch of 0.7 cm and were supported by a high strength epoxy cement plate. This plate consisting of vertically arrayed tubes is placed between the air plenum and the water column. The bubble generator produces uniform size bubbles. These bubbles get trapped in the air chamber and then a larger bubble escapes from the horizontal section which then smoothly rises into the test section as a cap bubble. Depending on the gas injection rates various sizes and frequencies of the cap bubbles were obtained. Demineralized water was used for the experiment. The four sensor probe was mounted on the traversing mechanism made of a micrometer screw gauge. In the present measurements the probe was stationed at 1.1 m from the inlet of the test section. Using the traversing mechanism, the probe center can be moved radially from the center towards the pipe wall up to 2.5 mm from the wall. A camera was mounted slightly upstream of the probe station. A strobe lighting system giving exposure of a few microseconds was used along with a Nikon camera system for still photography. For video photography a Panasonic PV510 camcorder was used with a shutter speed of 1 ms. In order to remove pipe curvature effects on the photography the test section was mounted with a water jacket providing a planar surface perpendicular to the direction of camera/video face. The data acquisition system consisted of a fast A/D converter Metrabyte DAS-20 board and a DELL 386/25 personal computer. The DAS-20 is capable of handling 100 000 samples per second. A manometer connected across the length of the test pipe gives an accurate measurement of two-phase pressure drop in the test section. This can be converted into two-phase gravitational head to obtain the global void fraction data. The liquid in the test pipe was stagnant, hence no net liquid flow occurs. Note, under the present experimental conditions the frictional loss was almost completely negligible in comparison with the head loss.

## 5. EXPERIMENTAL RESULTS AND DISCUSSION

The data were obtained using the four sensor probe for the cap bubbly flow regime at a superficial gas velocity range of 0.006–0.041 m $s^{-1}$. For this gas flow range the cap bubbles obtained were smooth and isolated from the small bubbles that follow the cap bubble. This enabled one to distinguish the cap and small bubbles during the data processing. Hence the separate measurements of the void fraction and the interfacial area concentration for the cap and the small bubbles was possible with the four sensor probe. The size of the cap bubbles in terms of diameter did not vary much. However, the length of the cap bubbles varied from 2.2 to 3.4 cm depending on the gas flow rate. With an increase in the gas flow rate the number of the small follow-up bubbles increased. The cap bubble frequency increased with an increase in the gas velocity.

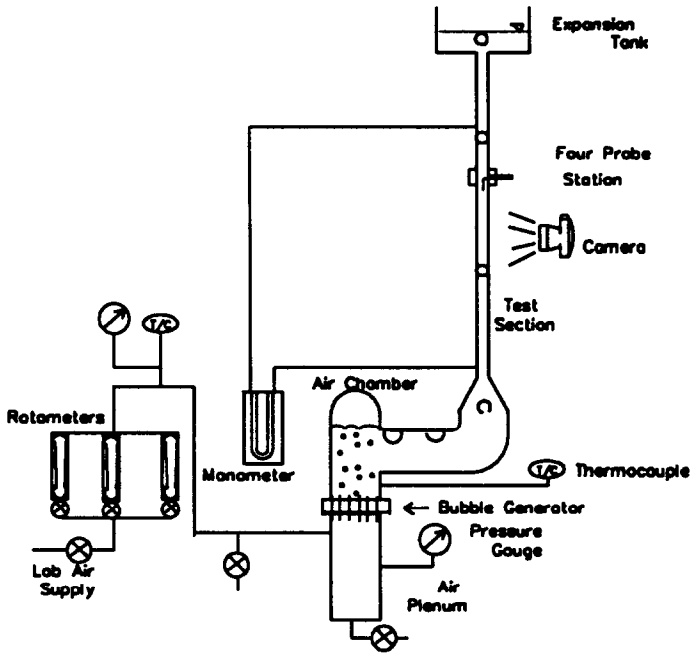


FIG. 3. Schematic of vertical air–water two-phase flow loop.

The void fraction measurements were obtained from the front sensor which defines the radial position of the four sensor probe in the pipe. The radial profiles of the void fraction at different gas flow rates for the cap bubbles are shown in Fig. 4(a). The shape of the profile resembles that of the cap bubble. With an increase in the gas flow rate higher void fractions were observed. The radial total void fraction profiles that include the contribution from cap bubbles and the follow-up small bubbles are shown in Fig. 4(b). The shape of the total void fraction profiles are similar to the cap bubble void fraction profiles. This indicates that the contribution from the cap bubbles to the void fraction is larger compared with the follow-up small bubbles. The visual observations (video and still photography) showed that the small bubbles moved behind the wake of the cap bubbles with approximately the same velocity as the tail velocity of the cap bubble. Hence it is assumed here that the small bubble velocity is the same as that of the tail velocity of the cap bubble. With this assumption it is observed that at low gas flow rate ($j_g \leqslant 0.02\ \mathrm{m\ s^{-1}}$) the radial profiles of the small bubble void fraction have a maximum at the pipe center with the diminishing value at the pipe wall. At high gas flow rate ($j_g \geqslant 0.04\ \mathrm{m\ s^{-1}}$) the small bubble profile is uniform across the cross section of the pipe except near the pipe wall.

The cap bubble void fraction profiles and the total void fraction profiles were area averaged in the radial direction using an area weighted average for each gas

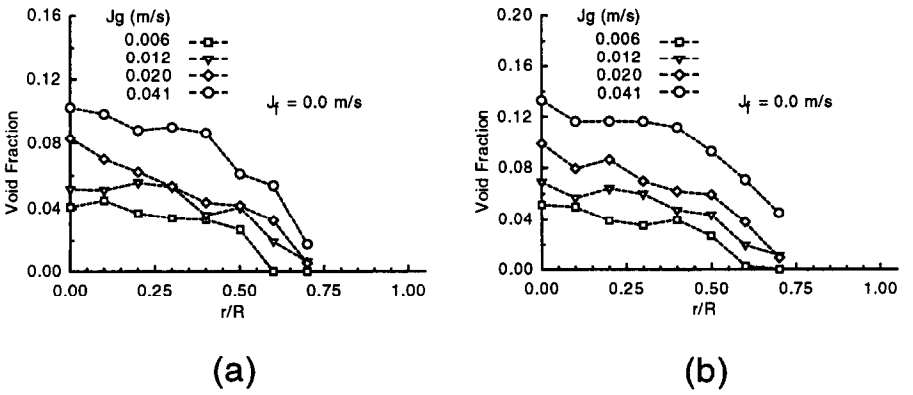


FIG. 4. Void fraction profiles of (a) cap bubbles and (b) cap and small bubbles at different gas flow rates.

flow rate. In Fig. 5(a) the average void fraction for the cap bubble and for total bubbles are shown as a function of superficial gas velocity. From this figure it is seen that with an increase in the gas flow rate the rate of increase in total average void fraction is large compared with that due to cap bubbles. This indicates that more smaller bubbles were observed with higher gas flow rate. This agrees with the visual observations. The average total void fraction obtained from the four sensor probe was compared with the global measurement. The global void fraction was obtained with the differential pressure (DP) measurement. Fig. 5(b) shows the comparison between the four probe and DP data. The agreement between the two measurements is very good.

The interfacial area concentration for the cap bubbles was calculated using the relations given by equations (17) and (18). The velocity components $v_{skj}$, $k = 1, 2, 3$ appearing in equation (17) were obtained both for the front and tail surfaces of each $j$th cap bubble. Then the interfacial area concentration contribution from front and tail surfaces were each added to get the net interfacial area concentration for each cap bubble. For the case of an interface of the cap bubble not detected by one of the rear sensors the interfacial area concentration was calculated using equation (21) as explained in Section 3.3. For small bubbles detected following a cap bubble, the tail velocity components obtained for that cap bubble was used as the mean harmonic velocity. The reciprocal of this mean harmonic velocity was then used to calculate the interfacial area concentration for the small bubble with the relation given by equation (8). Since each bubble has two surfaces the time interval $\tau$ is equal to $1/2N_t$, where $N_t$ is the number of small bubbles detected per unit time. The interfacial area for small bubbles estimated this way agreed well with the photographic and double probe method [9] used in our laboratory with error less than 7%. This uncertainty is due to the statistical nature of the small bubble velocity distribution.

In Fig. 6(a) the interfacial concentration profiles for cap bubbles at different gas flow rates are shown. The profiles show a higher interfacial area concentration near the larger curvature of the bubble. Thus the profiles show almost a mirror image of the cap bubble void fraction profile. The total interfacial area concentration that includes the contribution from cap and small bubbles is shown in Fig. 6(b). These profiles show almost a flat profile for the range of radial probe positions except for high gas flow rate at which a maxima is seen near half way between the pipe wall and center line. Due to the finite probe size the measurement near the pipe wall is not possible. However, near the pipe wall the value of interfacial area concentration should go down asymptotically to zero. The larger values of the interfacial area concentration observed (Fig. 6(b)) for the total cap and small bubbles indicates that the contribution from the small bubbles is quite substantial. This observation is not surprising since there are a large number of small bubbles and the ratio of surface area to volume is large for small bubbles compared with the cap bubbles.

The observation of the interfacial area concentration profiles indicates that the existence of a large number of small bubbles has a major effect in the cap or slug flow regime. Especially for slug flow in a vertical pipe which occurs following a flow regime transition from bubbly flow, the interfacial area concentration will be largely determined by the small bubble distribution.

A number of photographs of cap bubbles were used to analytically calculate the radial profiles of the void fraction and the interfacial area concentration. The method of this theoretical calculation of void fraction and interfacial area concentration is given in Appendix B. Basically eight to ten photographs of the cap bubbles were used to obtain the average representative cap bubble contour for each gas flow rate. The bubble contours were then fitted with fourth order polynomial expressions, where bubble height was related to the radial position from the pipe center line. Using

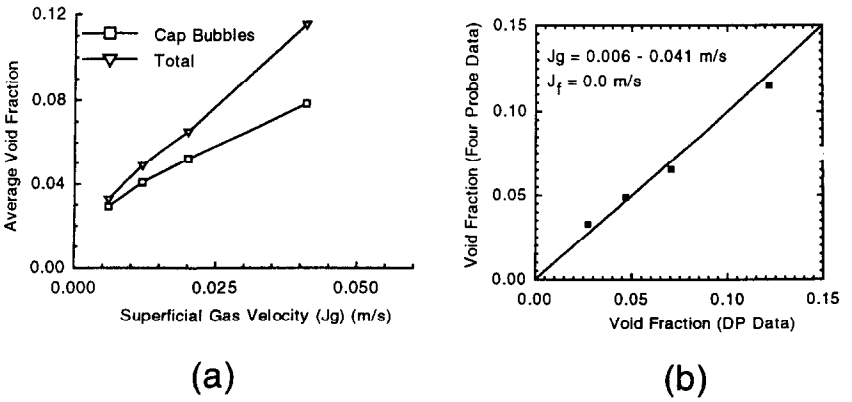


FIG. 5. Average void fraction (a) as a function of superficial gas velocity, (b) comparison with differential pressure measurement.

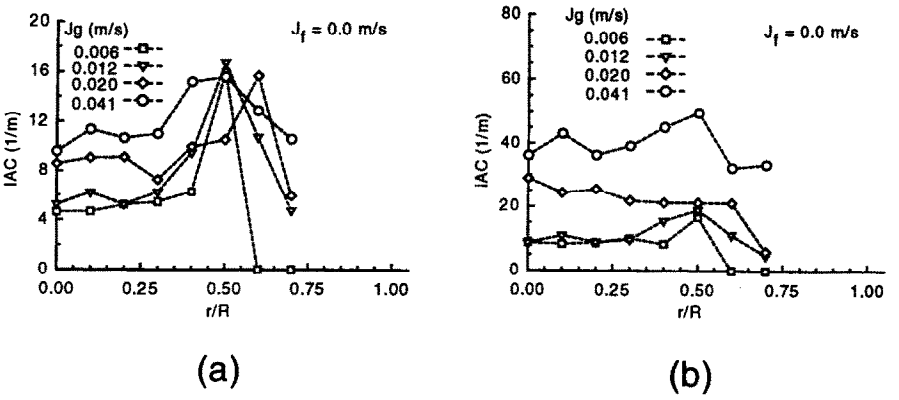


FIG. 6. Profiles of interfacial area concentration for (a) cap bubbles and (b) cap and small bubbles at different gas flow rates.

these expressions the void fraction and the interfacial area concentration profiles for the cap bubbles were obtained.

In Fig. 7 the comparison between the theoretical profile and the four sensor data for the void fraction is shown. The profile shapes of the four sensor data and the theoretical profiles are similar. The agreement in void fraction values is very good except for the gas flow rate at 0.02 m $s^{-1}$. At this gas flow rate some of the cap bubbles obtained had inclined or hollowed tail interfaces. In the theoretical calculation the cap bubble tail shape was taken as flat. It is possible that the bubble length used in the theoretical calculation is overestimated and hence the theoretical void fraction becomes too large.

The comparison between the theoretical interfacial area concentration profiles and four probe data is shown in Fig. 8. Though the values of the theoretical interfacial area concentration are lower than the four probe data near the center line of the pipe, the agreement between the two is acceptable. The reason for low values of the theoretical interfacial area concentration is attributed to the fact that a smooth contour was used for the bubble shape and the tail of the cap bubble was taken as flat. However, the cap bubbles in general have surface waves and the tail shape generally is quite irregular. These factors contribute to a higher interfacial area concentration measured with the four probe. The peaking of the interfacial area concentration near the wall region is clearly observed both in the data and the theoretical prediction. The area averaged void fraction and interfacial area concentration values obtained with the four probe and the theoretical profiles are compared in Fig. 9. Accounting for the theoretical underestimation of the interfacial area concentration, it can be said that agreement between the four sensor data and the theory is good. This establishes the reliability of using the four sensor proble to measure interfacial area concentration for cap or slug bubbles.

## 6. CONCLUSIONS

A theoretical formulation for the local measurement of interfacial area concentration in bubbly and cap bubbly flow using four sensor probe is discussed. The principles of using the four sensor electrical resistivity probe in bubbly or slug bubbly two-phase flow system including its design and signal processing are presented. Experimental data on void fraction and interfacial area concentration profiles are presented. The void fraction profiles for cap bubbles resembled the cap bubble shapes. The shapes of the total bubble void fraction profiles were similar to the cap bubble void fraction profiles indicating that the main contribution to the void fraction is from the cap bubbles.

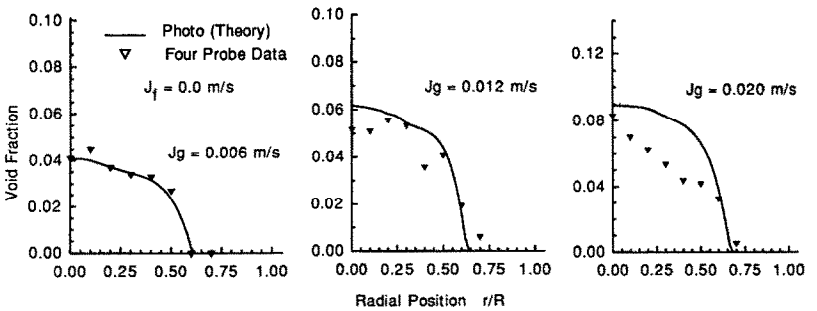


FIG. 7. Comparison of theoretical cap bubble void fraction profile with four sensor probe data.

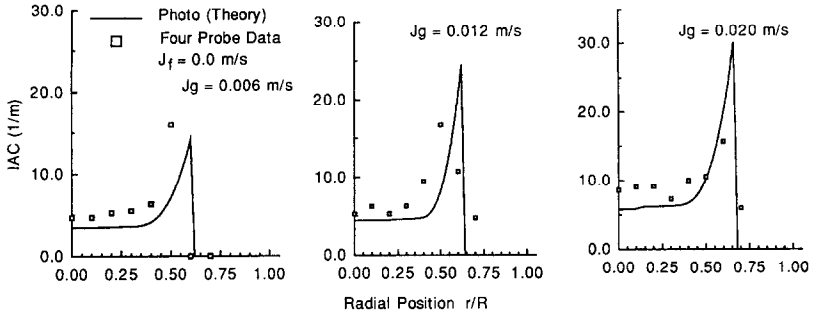


FIG. 8. Comparison of theoretical cap bubble interfacial area concentration profile with four sensor data.

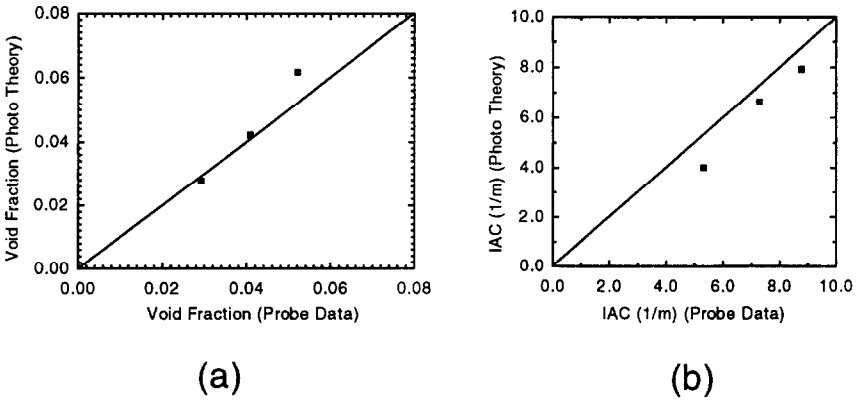


FIG. 9. Comparison of average theoretical cap bubble (a) void fraction and (b) interfacial area concentration with four sensor probe data.

The area averaged void fraction data obtained from the four sensor probe compared very well with the differential pressure measurements.

The interfacial area concentration profiles for the cap bubbles showed a higher interfacial area concentration near the larger curvature of the cap bubble. The four sensor probe data showed that in the presence of a large number of small bubbles in a cap or slug bubbly flow the interfacial area concentration is largely determined by the small bubbles.

Using the pictures of the cap bubbles, theoretical void fraction and interfacial area concentration for the cap bubbles were obtained. The theoretical void fraction and the interfacial area concentration profiles compared fairly well with the data obtained from the four sensor probe.

*Acknowledgements*—This work was performed under the auspices of U.S. Department of Energy, Office of Basic Energy Science. The authors would like to express their sincere appreciation for the encouragement, support and technical comments on this program from Dr O. P. Manley of DOE/BES.

## REFERENCES

1. M. Ishii, *Thermo-fluid Dynamic Theory of Two-phase Flow*. Eyrolles, Paris, Scientific and Medical Publication of France, New York (1975).
2. J. M. Delhaye, Equations fondamentales des ecoulements disphasiques, Parts 1 and 2, CEA-R-3429, France (1968).
3. H. K. Park and J. K. Yoon, A study on measurement of gas–liquid interfacial area in a dispersed gas injection system, *Metall. Trans. B* **21B,** 665–675 (1990).
4. I. Kotaoka, M. Ishii and A. Serizawa, Local formulation of interfacial area concentration, *Int. J. Multiphase Flow* **12,** 505–529 (1986).
5. I. Kataoka, M. Ishii and A. Serizawa, Local formulation of interfacial area concentration and its measurements in two-phase flow, Argonne National Laboratory Report, ANL-84-68, NUREG/CR-4029 (1984).
6. L. G. Neal and S. G. Bankoff, A high resolution resistivity probe for determination of local void properties in gas–liquid flow, *A.I.Ch.E. Jl* **9,** 490–494 (1963).
7. I. Kataoka and A. Serizawa, Averaged bubble diameter and interfacial area in bubbly flow, *Proceedings of the 5th Two-Phase Symposium of Japan*, Kobe, Japan, pp. 77–80, (28–29 Nov.) (1984).
8. Z. Wang and Kocamustafaogullari, Interfacial characteristic measurements in a horizontal bubbly two-phase flow, *ANS Trans.* **62,** 712–713 (1990).
9. S. T. Revankar and M. Ishii, Local interfacial area measurement in bubbly flow, *Int. J. Heat Mass Transfer* **35,** 913–925 (1992).
10. J. M. Burgess and P. H. Calderbank, The measurement of bubble parameters in two-phase dispersions—I. The development of an improved probe technique, *Chem. Engng Sci.* **30,** 743–750 (1975).
11. J. M. Burgess and P. H. Calderbank, The measurement of bubble parameters in two-phase dispersions—II. The structure of sieve tray froths, *Chem. Engng Sci.* **30,** 1107–1121 (1975).

12. J. M. Burgess and P. H. Calderbank, The measurement of bubble parameters in two-phase dispersions—III. Bubble properties in a freely bubbling fluidized-bed, *Chem. Engng Sci.* **30**, 1511–1518 (1975).
13. R. Buchholz, J. Tsepetonides, J. Steinemann and U. Onken, Influence of gas distribution on interfacial area and mass transfer in bubble columns, *Ger. Chem. Engng* **6**, 105–113 (1983).
14. I. Kataoka and A. Serizawa, Interfacial area concentration in bubbly flow, *Nucl. Engng Design* **120**, 163–180 (1990).

## APPENDIX A. DIRECTION COSINES FOR THE SENSOR TIPS

Consider Fig. A.1(a), where the location of the four sensors are shown with respect to a Cartesian coordinate system. The direction of the two-phase flow is parallel to the direction normal to the plane of the paper. The probe location in the test pipe is defined by the location of the front sensor which is the origin of the Cartesian coordinate system in Fig. A.1(a). The front sensor is denoted as 1 and the other three rear sensors as 2, 3 and 4. The line joining sensor tips 1 and 3 is taken in the direction parallel to the $y$-coordinate while sensor tips 3 and 4 are taken in the $xz$-plane. The distances between the front sensor 1 and the three rear sensors are given as $d_{12}$, $d_{13}$ and $d_{14}$. The distances between the rear sensors are $d_{23}$, $d_{24}$ and $d_{34}$.

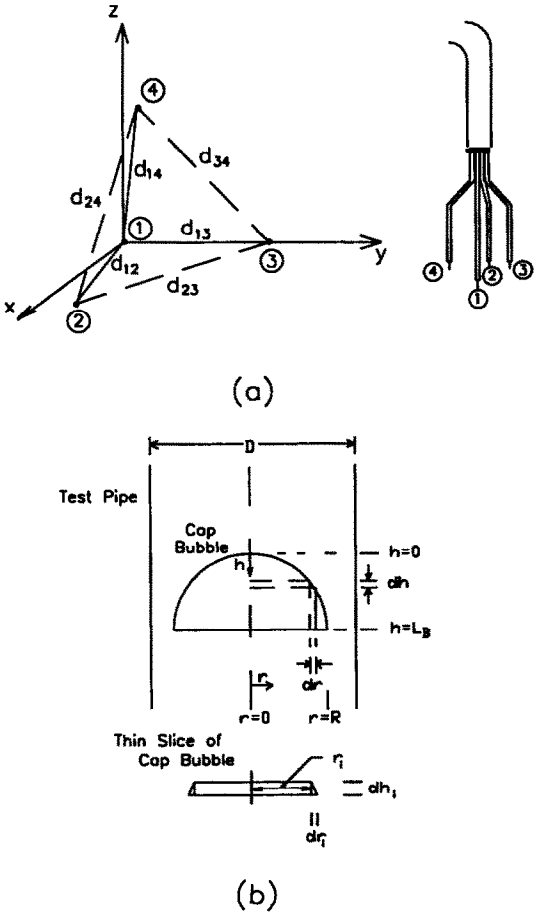


FIG. A.1. (a) Location of probe sensors with respect to Cartesian coordinate system, (b) Average cap bubble geometry for theoretical calculation of void fraction and interfacial area concentration.

Then the coordinates of the sensor tip $k$ are given as $(x_k, y_k, z_k)$, where $k = 1, 2, 3, 4$. The values of the $x_k$, $y_k$ and $z_k$ are given by the following relations:

$$x_1 = 0, \quad y_1 = 0, \quad z_1 = 0,$$

$$x_2 = \sqrt{(X^2 - z_2^2)}, \quad y_2 = \frac{d_{13}^2 - d_{23}^2 + d_{12}^2}{2d_{13}}, \quad z_2 = \frac{Y \cdot y_2 - Z^2 - Y^2}{Z}$$

where

$$X = \sqrt{(d_{12}^2 - y_2^2)}, \quad Y = \frac{y_4 D}{d_{14}}, \quad Z = \frac{z_4 D}{d_{14}},$$

$$D = \frac{d_{14}^2 - d_{24}^2 + d_{12}^2}{2d_{14}},$$

$$x_3 = 0, \quad y_3 = d_{13}, \quad z_3 = 0,$$

$$x_4 = 0, \quad y_4 = \frac{d_{13}^2 - d_{34}^2 + d_{14}^2}{2d_{13}}, \quad z_4 = \sqrt{(d_{14}^2 - y_4^2)}.$$

Now the direction cosines of the rear sensor $k$ are $(X_k, Y_k, Z_k)$, and given by the following relations

$$X_2 = \frac{x_2}{d_{12}}, \quad Y_2 = \frac{y_2}{d_{12}}, \quad Z_2 = \frac{z_2}{d_{12}},$$

$$X_3 = \frac{x_3}{d_{13}} = 0, \quad Y_3 = \frac{y_3}{d_{13}} = 1, \quad Z_3 = \frac{z_3}{d_{13}} = 0,$$

$$X_4 = \frac{x_4}{d_{14}} = 0, \quad Y_4 = \frac{y_4}{d_{14}}, \quad Z_4 = \frac{z_4}{d_{14}}.$$

## APPENDIX B. THEORETICAL CALCULATION OF INTERFACIAL AREA CONCENTRATION AND VOID FRACTION

For the theoretical calculation of the interfacial area concentration and the void fraction of the cap bubbles, the bubble pictures were used. Typical bubble pictures of the cap bubble were used for this purpose. First the cap bubble pictures taken at the same gas flow rate and having the same magnification were chosen. These were then traced on single tracing paper with a common test pipe center line and the same front elevation level for all the bubbles. Between eight and ten such pictures were used for each gas flow rate. Using these tracings of the cap bubble contours, a composite contour symmetric with the pipe center line was produced to represent the average cap bubble. The area and the length of each cap bubble contour was considered to get the average cap bubble contour.

Then the contour of the average cap bubble was fitted with a fourth order polynomial expression, where the bubble height was related to the radial position from the pipe center line. The bubble height was represented by the following equation (see Fig. A.1(b)):

$$h(r) = b_1 + b_2 r + b_3 r^2 + b_4 r^3 + b_5 r^4,$$

with $h = 0$ at $r = 0$ and $h = L_B$ at $r = R$.

The local void fraction is given by:

$$\alpha(r) = \left[1 - \frac{h(r)}{L_B}\right] N_t \frac{L_B}{V_b},$$

where $N_t$ and $V_b$ are cap bubble frequency and the velocity respectively.

The local interfacial area concentration is given as

$$a_i(r) = \left[\sqrt{\left[\left(\frac{dh}{dr}\right)^2 + 1\right]} + 1\right] \frac{N_t}{V_b}.$$